EPJ manuscript No.
(will be inserted by the editor)

An analytic parametrization of the hypernuclear matter equation of state

Hristijan Kochankovski[1], Àngels Ramos[1] and Isaac Vidaña[2]

[1] Departament de Física Quàntica i Astrofísica and Institut de Ciències del Cosmos, Universitat de Barcelona, Martí i Franquès 1, E-08028 Barcelona, Spain
[2]Istituto Nazionale di Fisica Nucleare, Sezione di Catania. Dipartimento di Fisica "Ettore Majorana", Università di Catania, Via Santa Sofia 64, I-95123 Catania, Italy

Received: date / Revised version: date

Abstract. An analytic parametrization of the cold hypernuclear matter a equation of state based on microscopic Brueckner–Hartree–Fock calculations is constructed using realistic nucleon-nucleon and hyperon-nucleon interactions. The parametrization is based on a simple phase-space analysis and reproduce with good accuracy the results of the microscopic calculations with a small number of parameters. This parametrization allow for rapid calculations that accurately mimic the microscopic results, being therefore, very useful from a practical point of view. As an example of its application we determine the composition, equation of state of neutron stars and some properties such as mass-radius relation, tidal deformability and moment of inertia using the equation of state derived from this parametrization.

PACS. 13.75.Ev Hyperon-nucleon interactions

1 Introduction

Neutron stars offer an interesting interplay between nuclear processes and astrophysical observables [1–4]. Properties of neutron stars, such as their masses, radii relationship, moment of inertia, crust thickness or cooling rates, are closely related to the underlying nuclear matter equation of state (EoS) for a wide range of densities and temperatures [5]. Thus its determination is an essential ingredient for understanding such properties.

At densities near the saturation density of nuclear matter, neutron star matter is thought to be mainly composed of neutrons, protons and leptons (electrons and muons) in equilibrium with respect to weak interaction processes (β-stable matter). As the density increases, new hadronic degrees of freedom may appear in addition to nucleons. Hyperons, baryons with a strangeness content, are an example of such additional degrees of freedom. Contrary to terrestial conditions, where hyperons are unstable and decay into nucleons through the weak interaction, the equilibrium conditions in neutron stars can make the inverse process, *i.e.,* the conversion of nucleons into hyperons, happen, so the formation of hyperons becomes energetically favorable. Although hyperonic matter is an idealized physical system, the theoretical determination of the corresponding EoS is an essential step towards the understanding of properties of neutron stars. Moreover, the comparison of theoretical predictions for the properties of these objects with the observations can provide strong constraints on the interactions among their constituents. Since the pioneering work of Ambartsumyan and Saakyan [6] the EoS of hyperonic matter has been considered by several authors either from phenomenological [7–16] or microscopic [23–36] approaches.

In phenomenological approaches the input is a density-dependent interaction which contains a certain number of parameters adjusted to reproduce experimental data. Within this approach Balberg and Gal [7] derived an analytic effective EoS using density-dependent baryon-baryon potentials based on Skyrme-type forces including hyperonic degrees of freedom. The features of this EoS rely on the properties of nuclei for the nucleon-nucleon (NN) interaction, and mainly on the experimental data from hypernuclei for the hyperon-nucleon (YN) and hyperon-hyperon (YY) interactions. This EoS reproduces characteristic properties of high-density matter found with theoretical microscopic models. Within the same scheme, several authors [17–22] have developed Skyrme-like YN potentials to study properties of single- and multi-Λ hypernuclei within the Skyrme–Hartree–Fock formalism.

An alternative phenomenological approach involves the formulation of an effective relativistic mean field theory (RMFT) of interacting hadrons [37, 38]. This fully relativistic approach treats the baryonic and mesonic degrees of freedom explicitely, and is, in general, easier to handle because it only involves local densities and fields. The EoS of dense matter with hyperons was first described within the RMFT by Glendenning [9–12] and latter by other authors [13–16]. The parameters in this approach are fixed by the properties of nuclei and nuclear bulk matter for

the nucleonic sector, whereas the coupling constants of the hyperons are fixed by symmetry relations, hypernuclear observables and compact star properties.

In microscopic approaches, on the other hand, the input are two-body baryon-baryon interactions that describe the scattering observables in free space. These realistic interactions have been mainly constructed within the framework of a meson-exchange theory, although recently a new approach based on chiral perturbation theory has emerged as a powerful tool. In order to obtain the EoS one has to solve the complicated nuclear many-body problem [39, 40]. A great difficulty of this problem lies in the treatment of the repulsive core, which dominates the short-range be- havior of the interaction. Various methods have been considered to solve the nuclear many-body problem: the variational approach [41], the correlated basis function (CBF) formalism [42], the self-consistent Green's function (SCGF) technique [43, 44], or the Brueckner–Bethe–Goldstone (BBG) [45, 46] and the Dirac–Brueckner–Hartree–Fock (DBHF) theories [47–49]. Nevertheless, although all of them have been extensively applied to the study of nuclear matter, up to our knowledge, only the BBG theory in the Brueckner–Hartree–Fock (BHF) approximation [23–31], the DBHF one [32, 33], the $V_{low\,k}$ approach [34], and very recently the quantum Monte Carlo method [35, 36] have been extended to the hyperonic sector.

The microscopic approach is in general technically complex and very CPU-time consuming. Therefore, from a practical point of view, it would be interesting to have an analytic parametrization of the hyperonic matter EoS based on such approach that allow to mimic the microscopic results in a fast way with a small number of parameters. In the present work we will build a density functional for the EoS based on microscopic Brueckner—Hartree–Fock (BHF) calculations of hyperonic matter at zero temperature. We should mention here that an analytical parametrization of hynuclear matter BHF calculations at finite temperature was already constructed by Burgio, Schulze and Li in Ref. [50] to study the properties of protoneutron stars containing hyperons. The strategy followed by these authors in the construction of their parametrization is, however, different from the one adopted here which is based, as it said in the abstract and will be shown, on a simple analysis of the phase space. In addition to the nucleonic degrees of freedom here we will consider only Λ and Σ^- hyperons in the construction of our functional, the reason being that these two types of hyperons are the ones appearing first in calculations of β-stable neutron star matter based on microscopic approaches [23–36]. The other hyperons, $\Sigma^0, \Sigma^+, \Xi^0$ and Ξ^-, being heavier, either do not appear or only show up at very large densities in these microscopic calculations.

The manuscript is organized in the following way. The BHF approach of hypernuclear matter is briefly reviewed in Sec. 2 whereas the construction of the parametrization is described in detail in Sec. 3, and applied in Sec. 4 to determine the composition, EoS and properties of neutron stars such as the mass-radius relation, the tidal deformability and the moment of inertia. The manuscript is finished with a short summary presented in Sec. 5.

2 Brief review of the BHF approach of hypernuclear matter

The BHF approach starts with the construction of all baryon-baryon (nucleon-nucleon (NN) and hyperon-nucleon (YN) in the present case) G-matrices which describe the interaction between two baryons in the presence of a surrounding medium. The G-matrices are obtained by solving the well-known coupled-channel Bethe–Goldstone integral equation, written schematically as

$$G(\omega)_{B_1B_2,B_3B_4} = V_{B_1B_2,B_3B_4} + \sum_{B_iB_j} V_{B_1B_2,B_iB_j} \frac{Q_{B_iB_j}}{\omega - E_{B_i} - E_{B_j} + i\eta} G(\omega)_{B_iB_j,B_3B_4} \quad (1)$$

where the first (last) two subindices indicate the initial (final) two-baryon states compatible with a given value S of the strangeness, namely NN for $S = 0$ and YN for $S = 1$; V is the bare baryon-baryon (NN or YN) interaction, $Q_{B_iB_j}$ is the Pauli operator that prevents the intermediate baryons B_i and B_j from being scattered to states below their respective Fermi momenta, ω is the sum of the non-relativistic single-particle energies of the interacting baryons, and η is an infinitesimal positive quantity. We note here that, although we have considered only Λ and Σ^- hyperons in the construction of our parametrization of the EoS, the Σ^0 and Σ^+ hyperons have been also taken into account in the intermediate YN states when solving the Bethe–Goldstone equation. The interested reader is referred to Refs. [23–31] for computational details.

The single-particle energy of a baryon B_i is given by

$$E_{B_i}(\boldsymbol{k}) = M_{B_i} + \frac{\hbar^2 k^2}{2M_{B_i}} + \mathrm{Re}[U_{B_i}(\boldsymbol{k})] \ , \quad (2)$$

where m_{B_i} denotes the rest mass of the baryon, and the (complex) single-particle potential $U_{B_i}(k_{B_i})$ represents the average field "felt" by the baryon owing to its interaction with other baryons. In the BHF approximation, $U_{B_i}(\boldsymbol{k})$ is calculated through the "on-shell" G-matrix, and is given by

$$U_{B_i}(\boldsymbol{k}) = \sum_{B_j} \sum_{\boldsymbol{k}'} n_{B_j}(|\boldsymbol{k}'|) \times \left\langle \boldsymbol{k}\boldsymbol{k}' \left| G\left(\omega = E_{B_i}(\boldsymbol{k}) + E_{B_j}(\boldsymbol{k}')\right) \right| \boldsymbol{k}\boldsymbol{k}' \right\rangle_{\mathcal{A}} \ . \quad (3)$$

Here $n_{B_j}(|\boldsymbol{k}'|)$ is the occupation number of the baryon species B_j, and the index $\mathcal{A}$ indicates that the matrix elements are properly antisymmetrized when baryons B_i and B_j belong to the same isomultiplet. We note here that the so-called continuous prescription has been adopted for the single-particle potentials when solving the Bethe–Goldstone equation, since, as it was shown in Refs. [51, 52], the contribution to the baryon energy per particle from three-hole line diagrams is minimized in this prescription.

All the calculations carried out in this work have been performed with the realistic Argonne V18 (AV18) NN interaction [53] supplemented with a three-nucleon force of Urbana type [54], which, for the use in the BHF calculations, was reduced to a two-body density-dependent force by averaging over the spatial, spin, and isospin coordinates of the third nucleon in the medium [55–57]. This three-nucleon force contains two parameters that are fixed by requiring that the BHF calculation reproduces the energy and saturation density of the symmetric nuclear matter. The interested reader is referred to the works of Refs. [58–60] for a recent analysis of the use of three-nucleon forces in nuclear matter. The YN G-matrices have been constructed using the NSC97e hyperon-nucleon interaction model of the Nijmegen group [61]. The reason behind the choice of this models is that this model results in the best predictions for hypernuclear observables among the potentials constructed by the Nijmegen group. The hyperon-hyperon interaction as well as three-body forces involving hyperons, *i.e.,* forces of the type NNY, NYY, and YYY, have not been taken into account in the present work due to the large uncertainties still existing on them.

In order to solve Eqs. (1)–(3), one starts from a reasonable guess for the single-particle potentials and obtain initial values of the G-matrices from Eq. (1), which is solved in a partial wave basis including contributions up to a total angular momentum $J = 4$. Then, the new single-particle potential is computed from Eq. (3) and used as an input in Eqs. (1)–(2). This iteration procedure continues until a desired level of convergence is reached. Once a self-consistent solution of Eqs. (1)–(3) is obtained, the baryon energy per particle can be calculated simply as

$$\left(\frac{E}{A}\right)_B = \sum_{B_i}\sum_{\boldsymbol{k}} n_{B_i}(|\boldsymbol{k}|)\left(\frac{\hbar^2k^2}{2M_{B_i}} + \frac{1}{2}\mathrm{Re}[U_{B_i}(\boldsymbol{k})]\right) \equiv \frac{K}{A} + \frac{V}{A}\ , \tag{4}$$

where

$$\frac{K}{A} = \sum_{B_i}\sum_{\boldsymbol{k}} n_{B_i}(|\boldsymbol{k}|)\frac{\hbar^2k^2}{2M_{B_i}} \tag{5}$$

and

$$\frac{V}{A} = \sum_{B_i}\sum_{\boldsymbol{k}} n_{B_i}(|\boldsymbol{k}|)\frac{1}{2}\mathrm{Re}[U_{B_i}(\boldsymbol{k})] \tag{6}$$

are, respectively, the free Fermi gas and the correlation energy contributions to the baryon energy per particle, which are functions of the partial densities $\rho_n, \rho_p, \rho_\Lambda$ and ρ_{Σ^-} or, equivalently of the quantities

$$\rho = \rho_n + \rho_p + \rho_\Lambda + \rho_{\Sigma^-}\ , \tag{7}$$

$$Y = \frac{\rho_{\Sigma^-} + \rho_\Lambda}{\rho}\ , \tag{8}$$

$$\beta = \frac{\rho_n - \rho_p}{\rho_n + \rho_p}\ , \tag{9}$$

$$\alpha = \frac{\rho_{\Sigma^-} - \rho_\Lambda}{\rho_{\Sigma^-} + \rho_\Lambda}\ , \tag{10}$$

where ρ is the total baryon number density, Y the total hyperon fraction, β the usual isospin asymmetry parameter, and α gives the asymmetry between the Λ and Σ^- hyperons.

3 Construction of the parametrization

As the reader can immagine Brueckner-type calculations are very CPU-time consuming since, as said above, one has to solve a self-consistent set of coupled-channel equations for different strangeness sectors. Therefore, from a practical point of view, it would be very interesting and useful to characterize the dependence of the baryon energy per particle $(E/A)_B$ on the particle densities $\rho_n, \rho_p, \rho_\Lambda$ and ρ_{Σ^-} or, on ρ, Y, β and α in a simple analytical form. The free Fermi gas contribution is already analytic and reads

$$\begin{aligned}\frac{K}{A} &= \sum_{B_i=n,p,\Lambda,\Sigma^-}\frac{3}{5}\frac{\hbar^2k_{F_{B_i}}^2}{2M_{B_i}}\frac{\rho_{B_i}}{\rho} \\ &= \frac{3}{20}\hbar^2k_F^2\left[(1-Y)^{5/3}\left(\frac{(1+\beta)^{5/3}}{M_n} + \frac{(1-\beta)^{5/3}}{M_p}\right)\right. \\ &\left. + Y^{5/3}\left(\frac{(1-\alpha)^{5/3}}{M_\Lambda} + \frac{(1+\alpha)^{5/3}}{M_{\Sigma^-}}\right)\right],\end{aligned} \tag{11}$$

where $k_{F_{B_i}} = (3\pi^2\rho_{B_i})^{1/3}$ is the Fermi momentum of the baryon B_i, and we have defined $k_F \equiv (3\pi^2\rho/2)^{1/3}$. An idea of the possible terms appearing in the correlation energy contribution, V/A can be obtained from the following phase space analysis of the single-particle potentials, similar to the ones performed in Ref. [62] for isospin asymmetric nuclear matter and in Ref. [63] for spin-polarized isospin asymmetric nuclear matter. Replacing the matrix elements $\left\langle \boldsymbol{k}\boldsymbol{k}' \left| G\left(\omega = E_{B_i}(\boldsymbol{k}) + E_{B_j}(\boldsymbol{k}')\right)\right| \boldsymbol{k}\boldsymbol{k}'\right\rangle_{\mathcal{A}}$ by an average value $g_{B_iB_j}(\boldsymbol{k}, \rho, Y, \beta, \alpha)$, in the Fermi sphere with radius $k' \leq k_{F_{B_j}}$ and integrating over the corresponding Fermi sea, the single-particle potentials of the four baryon species under consideration can be written as

$$\begin{aligned} U_n(\boldsymbol{k}) &\sim g_{nn}\rho_n + g_{np}\rho_p + g_{n\Lambda}\rho_\Lambda + g_{n\Sigma^-}\rho_{\Sigma^-}\ , \\ U_p(\boldsymbol{k}) &\sim g_{pn}\rho_n + g_{pp}\rho_p + g_{p\Lambda}\rho_\Lambda + g_{p\Sigma^-}\rho_{\Sigma^-}\ , \\ U_\Lambda(\boldsymbol{k}) &\sim g_{\Lambda n}\rho_n + g_{\Lambda p}\rho_p\ , \\ U_{\Sigma^-}(\boldsymbol{k}) &\sim g_{\Sigma^- n}\rho_n + g_{\Sigma^- p}\rho_p\ , \end{aligned} \tag{12}$$

where we have omitted the dependence on $\boldsymbol{k}, \rho, Y, \beta$ and α in the average G-matrices to simplify the notation.

For small values of the hyperon fraction, the isospin asymmetry and the Λ-Σ^- asymmetry, one can neglect the depedence on Y, β and α of the G-matrices assuming $g_{B_iB_j}(\boldsymbol{k}, \rho, Y, \beta, \alpha) \sim g_{B_iB_j}(\boldsymbol{k}, \rho)$ and

$$\begin{aligned} g_{nn} &\approx g_{pp} \equiv g_1(\boldsymbol{k}, \rho)\ , \\ g_{np} &\approx g_{pn} \equiv g_2(\boldsymbol{k}, \rho)\ , \\ g_{n\Lambda} &\approx g_{\Lambda n} \approx g_{\Lambda p} \approx g_{p\Lambda} \equiv g_3(\boldsymbol{k}, \rho)\ , \\ g_{n\Sigma^-} &\approx g_{\Sigma^- n} \equiv g_4(\boldsymbol{k}, \rho)\ , \\ g_{p\Sigma^-} &\approx g_{\Sigma^- p} \equiv g_5(\boldsymbol{k}, \rho)\ . \end{aligned} \tag{13}$$

	a_i	b_i	c_i	d_i
V_1	23090	1.191	−23010	1.187
V_2	54.56	3.757	−72.12	0.5256
V_3	−157	0.7538	238.3	2.679
V_4	−1047	0.9701	955.4	0.9691
V_5	−2019	0.6446	2063	0.6577

Table 1. Set of parameters a_i, b_i, c_i and d_i characterizing the density dependence of the coefficients $V_i(\rho)$. The parameters c_i and d_i are dimensionless, whereas the units of the parameters a_i and b_i are MeV×fm^{3c_i} and MeV×fm^{3d_i}, respectively.

Note that the quantities $g_i(\boldsymbol{k},\rho)$ receive contributions from different isospin (I) and strangeness (S) channels. Whereas $g_1(\boldsymbol{k},\rho)$ receives contributions only from the isospin triplet and zero strangeness channel, $g_2(\boldsymbol{k},\rho)$ has in addition a contribution from the isospin singlet, $g_3(\boldsymbol{k},\rho)$ and $g_4(\boldsymbol{k},\rho)$ are, respectively, purely isospin 1/2 and 3/2 with strangeness -1, and $g_5\boldsymbol{k},\rho$ has contributions from boyh $I=1/2$ and $I=3/2$ with $S=-1$.

Using the set of Eqs. (12) and (13), the single-particle potentials can be written as

$$U_n(\boldsymbol{k}) \sim \frac{\rho(1-Y)}{2}\left[g_1(\boldsymbol{k},\rho)(1+\beta)+g_2(\boldsymbol{k},\rho)(1-\beta)\right] + \frac{\rho Y}{2}\left[g_3(\boldsymbol{k},\rho)(1-\alpha)+g_4(\boldsymbol{k},\rho)(1+\alpha)\right] \ , \quad (14)$$

$$U_p(\boldsymbol{k}) \sim \frac{\rho(1-Y)}{2}\left[g_2(\boldsymbol{k},\rho)(1+\beta)+g_1(\boldsymbol{k},\rho)(1-\beta)\right] + \frac{\rho Y}{2}\left[g_3(\boldsymbol{k},\rho)(1-\alpha)+g_5(\boldsymbol{k},\rho)(1+\alpha)\right] \ , \quad (15)$$

$$U_\Lambda(\boldsymbol{k}) \sim \rho(1-Y)g_3(\boldsymbol{k},\rho) \ , \quad (16)$$

$$U_{\Sigma^-}(\boldsymbol{k}) \sim \frac{\rho(1-Y)}{2}\left[g_4(\boldsymbol{k},\rho)(1+\beta)+g_5(\boldsymbol{k},\rho)(1-\beta)\right] \quad (17)$$

where the particle densities $\rho_n, \rho_p, \rho_\Lambda$ and ρ_{Σ^-} have been written in terms of ρ, β, Y and α. These equations predict a linear dependence of the single-particle potentials on the hyperon fraction, the isospin asymmetry and the asymmetry between Λ's and Σ^-'s. Deviations from the linear behavior are, however, expected at higher values of Y, β and α. These deviations have to be associated to the dependence of the average G-matrices on Y, β and α, which have been neglected in the present analysis (see the set of Eqs. (13)).

Now using Eqs. (14)-(17), and replacing the quantities $g_i(\boldsymbol{k},\rho)$ by their averages $\bar{g}_i(\rho)$ in the corresponding Fermi spheres, one can see, after integration, that the correlation

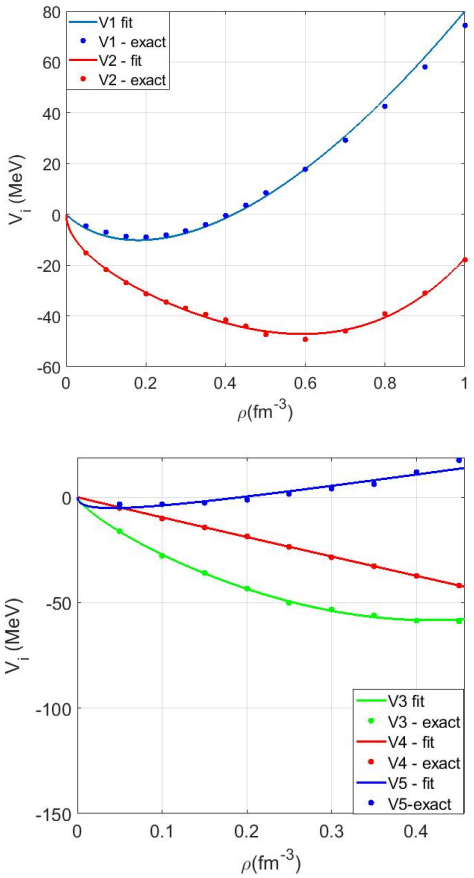

Fig. 1. Density dependence of the coefficients V_i. Solid circles show the result of the microscopic BHF calculation whereas solid lines refer to the power law fit of Eq. (21) with the parameters a_i, b_i, c_i and d_i given in Tab. 1 .

energy behaves like

$$\frac{V}{A} \sim \frac{\bar{g}_1(\rho)}{2\rho}(\rho_n^2+\rho_p^2)+\frac{\bar{g}_2(\rho)}{\rho}\rho_n\rho_p + \frac{\bar{g}_3(\rho)}{\rho}(\rho_n+\rho_p)\rho_\Lambda+\frac{\bar{g}_4(\rho)}{\rho}\rho_n\rho_{\Sigma^-} + \frac{\bar{g}_5(\rho)}{\rho}\rho_p\rho_{\Sigma^-} \ , \quad (18)$$

or replacing the particle densities in terms of ρ, β, Y and α

$$\frac{V}{A} \sim \frac{\rho}{4}\bar{g}_1(1-Y^2)(1+\beta^2)+\frac{\rho}{4}\bar{g}_2(1-Y^2)(1-\beta^2) + \frac{\rho}{2}\bar{g}_3Y(1-Y)(1-\alpha) + \frac{\rho}{4}\bar{g}_4Y(1-Y)(1+\alpha)(1+\beta) + \frac{\rho}{4}\bar{g}_5Y(1-Y)(1+\alpha)(1-\beta) \ . \quad (19)$$

From this simple analysis we can finally infer the form of

the correlation energy

$$\frac{V}{A} \sim V_1(\rho)(1-Y^2)(1+\beta^2) + V_2(\rho)(1-Y^2)(1-\beta^2) + V_3(\rho)Y(1-Y)(1-\alpha) + V_4(\rho)Y(1-Y)(1+\alpha)(1+\beta) + V_5(\rho)Y(1-Y)(1+\alpha)(1-\beta)\ . \quad (20)$$

The coefficients $V_1(\rho), \cdots, V_5(\rho)$ have been fitted to reproduce the microscopic BHF results corresponding to the following five set of values of Y, β and α:

$$(Y=0, \beta=0, \alpha=0)$$
$$(Y=0, \beta=1, \alpha=0)$$
$$(Y=0.1, \beta=0.875, \alpha=1)$$
$$(Y=0.15, \beta=0.7, \alpha=0.5)$$
$$(Y=0.14, \beta=0.4, \alpha=0.75)$$

in the density range $0.01\rho \leq \rho \leq 0.5$ fm^{-3}. The first two sets guarantee that the parametrization reproduces the microscopic results for symmetric and pure neutron matter. The other three have been chosen in order to mimic three representative β-stable matter compositions for densities above the hyperon threshold obtained with microscopic approaches (see *e.g.,* Refs. [23–36]). In addition, we have adjusted the density dependence of the coefficients $V_i(\rho)$ using a power law fit

$$V_i(\rho) = a_i \rho^{b_i} + c_i \rho^{d_i} \quad (21)$$

where the set of parameters a_i, b_i, c_i and d_i are given in Tab. 1. The coefficients V_ρ obtained from the microscopic (exact) BHF calculation together with the power law fit defined in Eq. (21) are show in Fig. 1 as a function of the density.

It is clear that the determination of these coefficients is not unique. However, we have checked that with the choice of this set of values of Y, β and α, we get a parametrization that reproduces with good quality the results of the BHF calculation for a wide range of arbitrary values of Y, β and α. This can be seen for instance in Fig. 2 where we compare the correlation energy for two different arbitrary compositions of hypernuclear matter obtained from the microscopic calculation (solid circles) and the parametrization (solid lines).

The main advantage of the parametrization of the baryon energy per particle just constructed is that it allows the analytical calculation of the chemical potential of the different baryons, needed to determine the equilibrium composition of neutron star matter, and of the baryon contribution to the pressure of the system.

The chemical potential of a given baryon B_i is determined from the partial derivative of the baryon energy density, $\varepsilon_B = \rho(E/A)_B$, of the system with respect the density ρ_{B_i} of the baryon

$$\mu_{B_i} = \frac{\partial \varepsilon_B}{\partial \rho_{B_i}} = M_{B_i} + \frac{\hbar^2 k_{F_{B_i}}}{2M_{B_i}} + \frac{\partial \varepsilon_{corr}}{\partial \rho_{B_i}}\ , \quad (22)$$

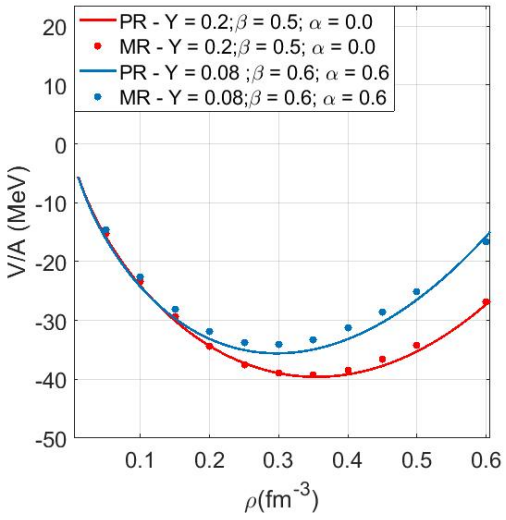

Fig. 2. Correlation energy for two different arbitrary compositions of hypernuclear matter. The solid circles show the microscopic results (MR) whereas those obtained with the parametrization (PR) are given by the solid lines.

where the mass of the baryon B_i, M_{B_i}, has been explicitly included in the definition of the chemical potential and $\varepsilon_{corr} = \rho(V/A)$ is the correlation energy density contribution. An analytic expression for the chemical potential of the different baryons can be simply obtained by using the parametrization derived for the correlation energy together with the set of Eqs. (7)-(10) to write

$$\frac{\partial \varepsilon_{corr}}{\partial \rho_{B_i}} = \frac{\partial \varepsilon_{corr}}{\partial \rho}\frac{\partial \rho}{\partial \rho_{B_i}} + \frac{\partial \varepsilon_{corr}}{\partial Y}\frac{\partial Y}{\partial \rho_{B_i}} + \frac{\partial \varepsilon_{corr}}{\partial \beta}\frac{\partial \beta}{\partial \rho_{B_i}} + \frac{\partial \varepsilon_{corr}}{\partial \alpha}\frac{\partial \alpha}{\partial \rho_{B_i}} \quad (23)$$

where

$$\frac{\partial \rho}{\partial \rho_{B_i}} = 1, \quad B_i = n, p, \Lambda, \Sigma^- \quad (24)$$

$$\frac{\partial Y}{\partial \rho_n} = \frac{\partial Y}{\partial \rho_p} = -\frac{Y}{\rho},\ \frac{\partial Y}{\partial \rho_\Lambda} = \frac{\partial Y}{\partial \rho_{\Sigma^-}} = \frac{1-Y}{\rho} \quad (25)$$

$$\frac{\partial \beta}{\partial \rho_n} = \frac{1-\beta}{\rho(1-Y)},\ \frac{\partial \beta}{\partial \rho_p} = -\frac{1+\beta}{\rho(1-Y)},\ \frac{\partial \beta}{\partial \rho_\Lambda} = \frac{\partial \beta}{\partial \rho_{\Sigma^-}} = 0 \quad (26)$$

$$\frac{\partial \alpha}{\partial \rho_n} = \frac{\partial \alpha}{\partial \rho_p} = 0,\ \frac{\partial \alpha}{\partial \rho_\Lambda} = -\frac{1+\alpha}{\rho Y},\ \frac{\partial \beta}{\partial \rho_{\Sigma^-}} = \frac{1-\alpha}{\rho Y} \quad (27)$$

and

$$\frac{\partial \varepsilon_{corr}}{\partial \rho} = v_1'(\rho)(1-Y^2)(1+\beta^2) + v_2'(\rho)(1-Y^2)(1-\beta^2) + v_3'(\rho)Y(1-Y)(1-\alpha) + v_4'(\rho)Y(1-Y)(1+\alpha)(1+\beta) + v_5'(\rho)Y(1-Y)(1+\alpha)(1-\beta) \quad (28)$$

$$\frac{\partial \varepsilon_{corr}}{\partial Y} = -2Yv_1(\rho)(1+\beta^2) - 2Yv_2(\rho)(1-\beta^2) + v_3(\rho)(1-2Y)(1-\alpha) + v_4(\rho)(1-2Y)(1+\alpha)(1+\beta) + v_5(\rho)(1-2Y)(1+\alpha)(1-\beta) \quad (29)$$

$$\frac{\partial \varepsilon_{corr}}{\partial \beta} = 2\beta v_1(\rho)(1-Y^2) - 2\beta v_2(\rho)(1-Y^2) + v_4(\rho)Y(1-Y)(1+\alpha) - v_5(\rho)Y(1-Y)(1+\alpha) \quad (30)$$

$$\frac{\partial \varepsilon_{corr}}{\partial \alpha} = -v_3(\rho)Y(1-Y) + v_4(\rho)Y(1-Y)(1+\beta) + v_5(\rho)Y(1-Y)(1-\beta) \quad (31)$$

with

$$v_i(\rho) = a_i\rho^{b_i+1} + c_i\rho^{d_i+1} \quad (32)$$

$$v_i'(\rho) = a_i(b_i+1)\rho^{b_i} + c_i(d_i+1)\rho^{d_i} \ . \quad (33)$$

The analytical expression for the baryon contribution to the pressure of the system can be simply obtained from the well-known thermodynamical relation

$$P_B = \rho^2 \frac{\partial((E/A)_B)}{\partial \rho} = \rho^2 \frac{\partial (K/A)}{\partial \rho} + \rho^2 \frac{\partial (V/A)}{\partial \rho} \quad (34)$$

where

$$\frac{\partial (K/A)}{\partial \rho} = \frac{\hbar^2 k_F^2}{10\rho}\left[(1-Y)^{5/3}\left(\frac{(1+\beta)^{5/3}}{M_n} + \frac{(1-\beta)^{5/3}}{M_p}\right) + Y^{5/3}\left(\frac{(1-\alpha)^{5/3}}{M_\Lambda} + \frac{(1+\alpha)^{5/3}}{M_{\Sigma^-}}\right)\right], \quad (35)$$

and

$$\frac{\partial (V/A)}{\partial \rho} = V_1'(\rho)(1-Y^2)(1+\beta^2) + V_2'(\rho)(1-Y^2)(1-\beta^2) + V_3'(\rho)Y(1-Y)(1-\alpha) + V_4'(\rho)Y(1-Y)(1+\alpha)(1+\beta) + V_5'(\rho)Y(1-Y)(1+\alpha)(1-\beta) \quad (36)$$

with

$$V_i'(\rho) = a_i b_i \rho^{b_i-1} + c_i d_i \rho^{d_i-1} \ . \quad (37)$$

4 Composition, EoS, and observables of neutron stars

As an application of the parametrization constructed, in this section we use it to determine the composition, the EoS and several observables of neutron stars. Adding to the baryon energy density ε_B and the pressure P_B the contribution from the noninteracting leptons, one can obtain the composition and the EoS of neutron star matter from the requirement of equilibrium under weak interaction processes:

$$\mu_i = b_i\mu_n - q_i\mu_e \quad (38)$$

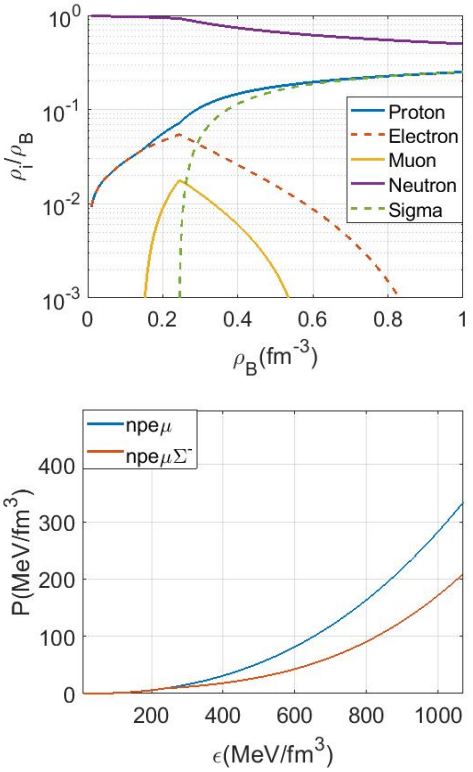

Fig. 3. Composition and EoS of neutron star matter. Upper panel: Particle fractions as a function of the total baryon density. Lower panel: pressure as a function of the total energy density.

where b_i and q_i denote, respectively, the baryon number and electric charge of the species i, and electric charge neutrality

$$\sum_i q_i\rho_i = 0 \ . \quad (39)$$

The composition and the EoS (pressure versus total energy density) obtained with the parametrization are respectively shown in the upper and lower panels of Fig. 3. The EoS is show for neutron star matter with and without hyperons. As seen in the figure, only Σ^- appears in the system leading to the deleptonization of the system. The reason for the lepton extinction is simple. They are relativistic particles which are "expensive" in terms of the energy of the system. Leptons are present in matter simply to guarantee electrical charge neutrality and, when it is energetically allowed, their role is played by the Σ^-, which in addition replaces also highly energetic neutrons. We should comment that although the Λ hyperon has been included in our calculations it does not appear because its chemical potential is always larger than that of the neutrons. This is in contrast with the microscopic BHF calculations, *e.g.,* of Refs. [28, 29] where the Λ also appears. The reason is probably due to the fact that in the present work we have used a three-nucleon force that is less repulsive than the ones employed in those works and, consequently, the neutron chemical potential does not rises enough to equal that of the Λ. As far as the EoS regards, as it is

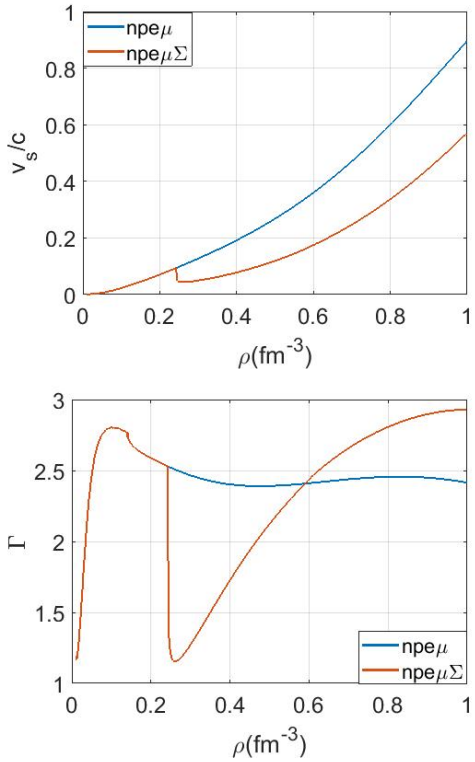

Fig. 4. Speed of sound (upper panel) and adiabatic index (lower panel) of neutron star matter with and without hyperons.

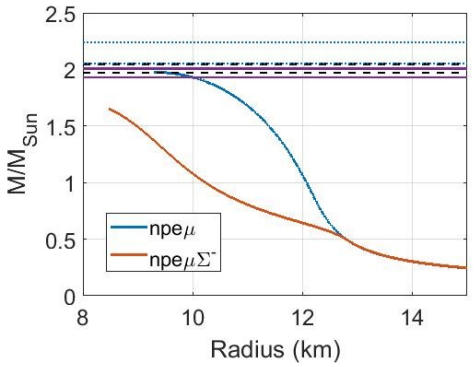

Fig. 5. Mass-radius relation for nucleonic and hyperionic. Horizontal violet, black and blue lines show the observational upper and lower limits inferred, respectively, from the mass measurements of PSR J1614-2230 ($1.928 \pm 0.017\,M_\odot$) [64] PSR J0348+0432 ($2.01 \pm 0.04\,M_\odot$) [65] and PSR J0740+6620 ($2.14^{+0.10}_{-0.09}\,M_\odot$) [66].

seen in the lower panel of the figure and it is well known, due to the presence of the Σ^- the pressure exerted by matter is relieved and, therefore, the EoS becomes softer. To further illustrate this softening, we show in Fig. 4 the speed of sound (upper panel) and so-called adiabatic index (lower panel),

$$\Gamma = \frac{\varepsilon}{P}\frac{\partial P}{\partial \varepsilon}\ , \tag{40}$$

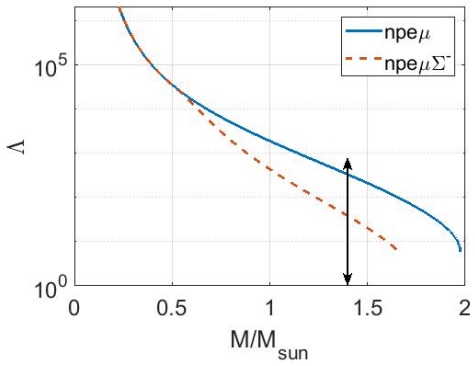

Fig. 6. Dimensionless tidal deformability for nucleonic and hyperonic stars. The double arrow shows the range of variation of the weighted-average dimensionless tidal deformability obtained from the analysis of the event GW170817 event [72–74].

for matter with and without hyperons. As it can be seen both quantities have a drop at the value of the onset density of the Σ^-. Note that, although the formalism employed is non-relativistic, causality is guarantee in the full range of densities considered thanks to the presence of the Σ^-.

We will now examine few neutron star observables. We start by showing in Fig. 5 the mass-radius relation obtained using our parametrization of the EoS with and without hyperons when solving the well-known Tolman–Oppenheimer–Volkoff (TOV) equations. The observational upper and lower limits inferred from the mass measurements of PSR J1614-2230 ($1.928 \pm 0.017\,M_\odot$) [64] PSR J0348+0432 ($2.01 \pm 0.04\,M_\odot$) [65] and PSR J0740+6620 ($2.14^{+0.10}_{-0.09}\,M_\odot$) [66] are also shown. As expected the softening of the EoS due to the presence of hyperons leads to a reduction of the neutron star mass and, particularly, of its maximum value which is clearly incompatible with the current observational constraints. This incompatibility together with the fact that the presence of hyperons in neutron star interiors seems to be energetically unavoidable is at the origin of the well-known "hyperon puzzle", a problem that is still open and whose solution is not easy. For a discussion of this problem and its possible solutions, the interested reader can see, *e.g.,* Refs. [67, 68] and references therein.

Gravitational waves (GW) originated during the coalescence of two neutron stars or a black hole and a neutron star constitute nowadays a new and valuable source of information on the EoS and internal structure os neutron stars. In particular, the so-called tidal deformability λ, or equivalently the tidal Love number $k_2 = \frac{3}{2}\frac{\lambda}{R^5}$ of a neutron star [69–71] can provide priceless information and constraints on the related EoS, because it depends strongly on the M/R ratio (*i.e.,* the compactness) of the star. The tidal deformability can be obtained by solving the TOV equations together with an additional differential equation (see Refs. [69–71] for details). We show in Fig. 6 the dimensionless tidal deformability $\Lambda = \lambda/M^5$ obtained using our parametrization for neutron stars with and without hyperons. The double arrow shows the range of variation

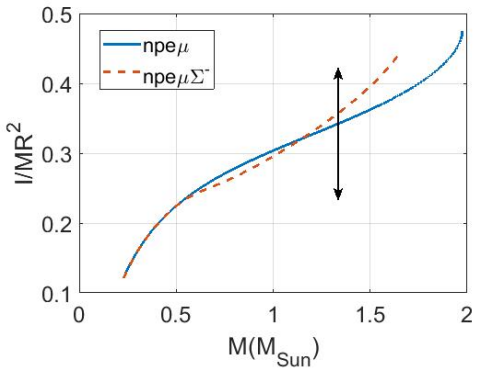

Fig. 7. Moment of inertia for nucleonic and hyperonic stars. The double arrow shows the bounds on the moment of inertia of the double pulsar PSR J0737-3039 [77] inferred from the GW170817 event .

of the weighted-average dimensionless tidal deformability obtained from the analysis of the event GW170817 event [72–74] originated from the merger of two neutron stars. Requiring both stars to have the same EoS leads to the constraints $70 < \Lambda_{1.4} < 580$ and $10.5 < R_{1.4} < 13.3$ km [73] for a $1.4\,M_\odot$ neutron star. Note that the prediction of Λ for a $\sim 1.4\,M_\odot$ nucleonic or hyperonic star is compatible with observation even if in the later case the maximum mass is smaller than $2\,M_\odot$.

To finish this section we show in Fig. 7 the moment of inertia of nucleonic and hyperonic stars which has been obtained by solving the structure a rotating neutron star using the Hartle–Thorne approach [75, 76]. The double arrow shows the bounds on the moment of inertia of the double pulsar PSR J0737-3039 [77] inferred from the analysis of the GW170817 event. As it is seen the moment of inertia of the nucleonic star rises initially almost when increasing the mass in the range $\sim 0.5\,M_\odot < M < 1.5\,M_\odot$. This trend, however, is broken for masses larger than $\sim 1.5\,M_\odot$ for which the moment of inertia increases much faster, and is not observed in the case of the hyperonic star in any mass range. We note that in both cases the predicted moment of inertia for a $1.4\,M_\odot$ is compatible with the observational values for PSR J0737-3039 obtained indirectly from the GW170817 event. However, we should point out that an independent measurement of the moment of inertia of a neutron star does not exist yet. Therefore, the compatibility of our results with this observational data has to be taken with care.

5 Summary

We have constructed an analytic parametrization of the hyperonic matter equation of state at zero temperature based on microscopic BHF calculations using the realistic Argonne V18 nucleon-nucleon potential plus a three-nucleon force of Urbana type and the NSC97e hyperon-nucleon interaction model of the Nijmegen group. Hyperon-hyperon interactions as well as three-body forces involving hyperons, have not been taken into account in the present work due to the large uncertainties still existing on them. The construction of this parametrization has been based on a simple phase-space analysis. We have shown that the parametrization reproduces with good accuracy the results of the microscopic calculations, allowing for rapid calculations that accurately mimic the microscopic BHF results being, thus, very useful from a practical point of view. As an example of its application we have determined the composition and EoS of neutron star matter as well as several properties of these objects such as their mass-radius relation, the tidal deformability and the moment of inertia. The results for the tidal deformability and the moment of inertia have been compared with observational data inferred from the analysis of the GW170817 event finding compatible values of both quantities with observation. Our parametrization will be extended in the near future to include finite temperature effects, necessary to describe the properties of newborn neutron stars, neutron star merger, and the conditions of matter in relativistic heavy-ion collisions.

Acknowledgements

This work has been supported by the COST Action CA16214 “PHAROS: The multi-messenger physics and astrophysics of neutron stars”.

References

1. S. L. Shapiro and S. A. Teukolsky, *Black Holes, White Dwarfs and Neutron Stars* (Wiley, New York, 1983).
2. N. K. Glendenning, *Compact Stars: Nuclear Physics, Particle Physics and General Relativity*, 2nd Ed. (Springer, Berlin, 2000).
3. P. Haensel, A. Y. Potekhin and D. G. Yakovlev, *Neutron Stars 1: Equation of State and Structure*, Astrophysics and Space Science Library, vol. **326**, (Springer, New York, 2007).
4. L. Rezzola, P. Pizzochero, D. I. Jones, N. Rea and I. Vidaña Eds., *The Physics and Astrophysics of Neutron Stars*, Astrophysics and Space Science Library, vol. **. 457** (Springer Nature, Switzerland, 2018).
5. N. Chamel and P. Haensel, Living Review on Relativity **11**, 10 (2008).
6. V. A. Ambartsumyan and G. S. Saakyan, Sov. Astron. **4**, 187 (1960).
7. S. Balberg and A. Gal, Nucl. Phys. A **625**, 435 (1997).
8. S. Balberg, I. Lichtenstadt and G. B. Cook, Astrophys. J. Suppl. Ser. **121**, 515 (1999).
9. N. K. Glendenning, Phys. Lett. B **114**, 392 (1982).
10. N. K. Glendenning, Astrophys. J. **293**, 470 (1985).
11. N. K. Glendenning, Z. Phys. A **326**, 57 (1987).
12. N. K. Glendening and S. A. Moszkowski, Phys. Rev. Lett. **67**, 2414 (1991).
13. F. Weber and M. K. Weigel, Nucl. Phys. A **505**, 779 (1989).
14. R. Knorren, M. Prakash and P. J. Ellis, Phys. Rev. C **52**, 3470 (1995).

15. J. Schaffner and I. Mishustin, Phys. Rev. C **53**, 1416 (1996).
16. H. Huber, F. Weber, M. K. Weigel and Ch. Schaab, Int. J. Mod. Phys. E **7**, 310 (1998).
17. D. E. Lanskoy and Y. Yamamoto, Phys. Rev. C **55**, 2330 (1997).
18. T. Y. Tretyakova and D. E. Lanskoy, Eur. Phys. J. A **5**, 391 (1999).
19. J. Cugnon, A. Lejeune and H.-J. Schulze, Phys. Rev. C **62**, 064308 (2000).
20. I. Vidaña, A. Polls, A. Ramos and H.-J. Schulze, Phys. Rev. C **64**, 044301 (2001).
21. X.-R. Zhou , H.-J. Schulze, H. Sagawa, C.-X. Wu and E.-G. Zhao, Phys. Rev. C **76**, 034312 (2007).
22. X.-R. Zhou, A. Polls, H.-J. Schulze and I. Vidaña, Phys. Rev. C **78**, 054306 (2008).
23. H.-J. Schulze, M. Baldo, U. Lombardo, J. Cugnon and A. Lejeune, Phys. Lett. B **355** 21 (1995);
24. H.-J. Schulze, M. Baldo, U. Lombardo, J. Cugnon and A. Lejeune, Phys. Rev. C **57**, 704 (1998).
25. M. Baldo, G. F. Burgio and H.-J. Schulze, Phys. Rev. C **58**, 3688 (1998).
26. M. Baldo, G. F. Burgio and H.-J. Schulze, Phys. Rev. C **61**, 055801 (2000).
27. I. Vidaña, A. Polls, A. Ramos, M. Hjorth-Jensen and V. G. J. Stoks, Phys. Rev. C **61**, 025802 (2000).
28. I. Vidaña, A. Polls, A. Ramos, L. Engvik and M. Hjorth-Jensen, Phys. Rev. C **62**, 035801 (2000).
29. H-J. Schulze, A. Polls, A. Ramos and I. Vidaña, Phys. Rev. C **73**, 058801 (2006).
30. H.-J. Shulze and T. Rijken, Phys. Rev. C **84**, 035801 (2011).
31. D. Logoteta, I. Vidaña and I. Bombaci, Eur. Phys. J. A **55**, 207 (2019).
32. F. Sammarruca, Phys. Rev. C **79** 034301 (2009).
33. T. Katayama and K. Saito, arXiv:1410.7166 (2014); arXiv:1501.05419 (2015).
34. H. Dapo, B.-J. Schaefer and J. Wambach, Phys. Rev. C **81**, 035803 (2010).
35. D. Lonardoni, F. Pederiva and S. Gandolfi, Phys. Rev. C **89** 014314 (2014).
36. D. Lonardoni, A. Lobato, A, Gandolfi and F. Pederiva, Phys. Rev. Lett. **114**, 092301 (2015).
37. B. D. Serot and J. D. Walecka, Adv. Nucl. Phys. **16**, 1 (1986).
38. B. D. Serot and J. D. Walecka, Int. J. Mod. Phys. E **6**, 515 (1997).
39. M. Baldo Ed., *Nuclear Methods and Nuclear Equation of State*. International Review of Nuclear Physics, vol.. **8** (World Scientific Publishing Company, 1999).
40. H. Müther and A. Polls, Prog. Part. Nucl. Phys. **45**, 243 (2000).
41. A. Akmal, V. R. Pandharipande and D. G. Ravenhall, Phys. Rev. C **58**, 1804 (1998).
42. A. Fabrocini and S. Fantoni, Phys. Lett. B **298**, 263 (1993).
43. L. P. Kadanof and G. Baym, *Quantum Statistical Mechanics* (Benjamin, New York, 1962)).
44. W. D. Kraeft, D. Kremp, W. Ebeling and G. Röpke, *Quantum Statistics of Charged Particle Systems* (Akademie-Verlag, Berlin, 1986).
45. K. A. Brueckner, S. A. Coon and J. Dabrowski, Phys,. Rev. **168**, 1184 (1968).
46. P. J. Siemens, Nucl. Phys. A **141**, 225 (1970).
47. B. ter Haar and R. Malfliet, Phys. Rep. **149**, 207 (1987).
48. B. ter Haar and R. Malfliet, Phys. Rev. C **36**, 1611 (1987).
49. R. Brockmann and R. Machleidt, Phys. Rev. C **42**, 1965 (1990).
50. G. F. Burgio, H.-J. Schulze, and A. Li, Phys. Rev. C **83**, 025804 (2011).
51. H. Q. Song, M. Baldo, G. Giansiracusa and U. Lombardo, Phys. Rev. Lett. **81**, 1584 (1998).
52. M. Baldo, G. Giansiracusa, U. Lombardo and H. Q. Song, Phys. Lett. B **473**, 1 (2000).
53. R. B. Wiringa, V. G. J. Stoks and R. Schiavilla, Phys. Rev. C **51**, 38 (1995).
54. J. Carlson, V. R. Pandharipande and R. B. Wiringa, Nucl. Phys. A **401**, 59 (1983).
55. A. Loiseau, Y. Nogami and C. K. Ross, Nucl. Phys. A **165**, 601 (1971).
56. P. Grangé, M. Martzolff, Y. Nogami, D. W. L. Sprung anc C. K. Ross, Phys. Lett. B **60**, 237 (1976).
57. M. Baldo and L. Ferreira, Phys. Rev. C **59**, 682 (1999).
58. X. R. Zhou, G. F. Burgio, U. Lombardo, H.-J. Schulze and W. Zuo, Phys. Rev. **69**, 018801 (2004).
59. Z. H. Li, U. Lombardo, H.-J. Schulze and W. Zuo, Phys. Rev. C **77**, 034316 (2008).
60. Z. H. Li and H.-J. Schulze, Phys. Rev. C **78**, 028801 (2008).
61. V. G. J. Stoks and Th. A. Rijken, Phys. Rev. C **59**, 3009 (1999).
62. I. Bombaci and U. Lombardo, Phys. Rev. C **44**, 1892 (1991).
63. I. Vidaña and I. Bombaci, Phys. Rev. C **66**, 045801 (2002).
64. P. Demorest *et al.,* Nature **467**, 1081 (2010).
65. J. Antoniadis *et al.,* Science **340**, 1233 (2013).
66. H. T. Cromartie *et al.,* Nature Astronomy **4**, 72 (2020).
67. D. Chatterjee and I. Vidaña, Eur. Phys. J. A **52**, 29 (2016).
68. I. Vidaña, Proc. R. Soc. A **474**, 0145 (2018).
69. T. Hinderer, Astrophys. J. **677**, 1216 (2008).
70. T. Hinderer, Astrophys. J. **697**, 964 (2009).
71. T. Hinderer, B. D. Lackey, R. N. Lang, and J. S. Read, Phys. Rev. D **81**, 123016 (2010).
72. B. P. Abbot *et al.,* Phys. Rev. Lett. **119**, 161101 (2017).
73. B. P. Abbot *et al.,* The LIGO Scientific Collaboration and the Virgo Collaborationn, Phys. Rev. Lett. **121**, 161101 (2018).
74. B. P. Abbot *et al.,* The LIGO Scientific Collaboration and the Virgo Collaboration, Phys. Rev. X **9**, 011001 (2019).

75. J. B. Hartle, Astrophys. J. **150**, 1005 (1967).
76. J. B. Hartle and K. S. Thorne, Astrophys. J. **153**, 807 (1968).
77. P. Landry and B. Kumar, Astrophys. J. **868**, L22 (2018).